THE GEOLOGICAL SOCIETY OF AMERICA®

Thermal equation of state for zoisite: Implications for the transportation of water into the upper mantle and the high-velocity anomaly in the Farallon plate

Shijie Huang[1,2], Zhilin Ye[1,2], Dawei Fan[1,†], Jingui Xu[3,†], Dongzhou Zhang[3], Wei Chen[1,2,4], Yunqian Kuang[1,2,5], and Wenge Zhou[1]

[1]*Key Laboratory of High-Temperature and High-Pressure Study of the Earth's Interior, Institute of Geochemistry, Chinese Academy of Sciences, Guiyang 550002, China*
[2]*University of the Chinese Academy of Sciences, Beijing 100049, China*
[3]*Hawai'i Institute of Geophysics and Planetology, School of Ocean and Earth Science and Technology, University of Hawai'i at Manoa, Honolulu, Hawaii, 96822 USA*
[4]*Guizhou Polytechnic of Construction, Guiyang 551400, China*
[5]*Bureau of Natural Resources and Planning of Yongzhou, Yongzhou 425000, China*

ABSTRACT

Seismic tomography studies have revealed a high-velocity anomaly at depths between 100 km and 300 km in the Farallon plate. However, the reasons for the high-velocity anomaly continue to be debated. An analysis of the mineral proportions of eclogites exhumed from the Farallon plate shows that the average amount of zoisite in eclogite is ~16.0 vol%. Therefore, the presence of zoisite eclogite needs to be considered to explain the high-velocity anomaly of the Farallon plate. However, the thermal equation of state and stability of zoisite have not been fully investigated under high pressure–temperature (*P-T*) conditions. We investigated the high-pressure and high-temperature behavior of natural zoisite utilizing synchrotron single crystal-X-ray diffraction (XRD). The results indicate that zoisite is metastable up to 24.8 GPa and 700 K. We obtained the ambient unit-cell volume $V_0 = 901.26(3)$ Å^3 by synchrotron single crystal-XRD measurement. We also fitted the pressure-volume-temperature data to a high-temperature Birch-Murnaghan equation of state and obtained the zero-pressure bulk modulus $K_0 = 134.7(8)$ GPa, the temperature derivative of the bulk modulus $(\partial K/\partial T)_P = -0.011(4)$ GPa/K, and the thermal expansion coefficients $\alpha_{0V} = 1.9(7) \times 10^{-5}$ K^{-1} and $\alpha_{1V} = 3(2) \times 10^{-8}$ K^{-2} when the pressure derivative of bulk modulus (K'_0) is fixed at 4. By incorporating the results from previous studies, we calculated the density and bulk sound velocity profiles of zoisite eclogite along the Farallon plate geotherm. Finally, we infer that zoisite could carry water to depths of ~300 km within cold subducting slabs and that the bulk sound velocity of typical zoisite eclogite with ~61.0 vol% omphacite, ~23.0 vol% garnet, and ~16.0 vol% zoisite could cause the high-velocity anomalies at depths of 100–300 km in the Farallon plate.

INTRODUCTION

There are many regions of velocity anomalies distributed in the Earth's interior (Roecker, 1982; Yang, 2009). Among them, the Farallon plate is a typical cold subduction slab in western North America, which is ~200 °C colder than the ambient upper mantle (Van der Lee and Nolet, 1997; English et al., 2003). Seismic tomography studies have indicated that a high-velocity anomalies region exists at depths between 100 km and 300 km along the northwest to southeast section of the Farallon plate (e.g., Van der Lee and Nolet, 1997; Levander et al., 2011; Pavlis et al., 2012; Wang et al., 2013). Moreover, previous studies have indicated that the high-velocity anomaly at depths of 100–300 km in the Farallon plate is 0.5%–4% (e.g., Sigloch, 2011; Wang et al., 2013). However, the explanations for the high-velocity anomaly remain a subject of debate. Proposed explanations include the distribution of high-Mg andesites, the temperature anomaly of the Farallon plate, and the structure of the tectonic plate and the dip of plate subduction (e.g., Van der Lee and Nolet, 1997; Levander et al., 2011; Pavlis et al., 2012; Wang et al., 2013).

Rock type also has an important effect on the bulk sound velocity. Eclogite is a key component of the Farallon plate (Usui et al., 2003). Normally, eclogite has a higher wave velocity than other rocks, such as peridotite, under the same pressure and temperature conditions (Urann et al., 2020). Among the rock-forming minerals of eclogite, zoisite is a typical secondary mineral in ultrahigh/high-pressure eclogite (for example, the Dabie-Sulu and Tibet ultrahigh-pressure metamorphic zones), and the content of zoisite is typically ~7 vol% in Dabie-Sulu (e.g., Zheng et al., 2007; Zhang et al., 2008; Liu et al., 2009; Liu et al., 2010; Zheng et al., 2011; Chen et al., 2014; Li et al., 2018; Feng et al., 2021) and ~10 vol% in Tibet (e.g., Li et al., 2009; Wei et al., 2009; Zheng, 2009; Xiao et al., 2012; Cheng et al., 2015; Dong et al., 2016; Zhang et al., 2016; Zhang et al., 2019). Moreover, the Farallon plate is also an important ultrahigh-pressure metamorphic zone, and the eclogite contains a high amount of zoisite. Specifically, the average amount of zoisite in the Farallon plate eclogite is ~16.0 vol%, and the maximum is ~41.4 vol% (e.g., Selverstone et al., 1999; Hacker and Abers, 2004; Zack et al., 2004; Usui et al., 2003, 2006, 2007; Marot et al., 2014; Hernández-Uribe and Palin, 2019; Bustamante et al., 2021).

Although most hydrous minerals have relatively lower sound velocities than anhydrous minerals, zoisite has a higher sound velocity than most hydrous minerals and some upper mantle anhydrous minerals (e.g., omphacite) in

†Corresponding authors: Dawei Fan (fandawei@vip.gyig.ac.cn); Jingui Xu (xujingui@hawaii.edu).

GSA Bulletin; May/June 2023; v. 135; no. 5/6; p. 1178–1186; https://doi.org/10.1130/B36479.1; 5 figures; 6 tables.
published online 25 August 2022

For permission to copy, contact editing@geosociety.org
© 2022 Geological Society of America

Downloaded from http://pubs.geoscienceworld.org/gsa/gsabulletin/article-pdf/135/5-6/1178/5827011/b36479.1.pdf
by Argonne National Laboratory user

subducting slabs (Mans et al., 2019). Therefore, the presence of zoisite eclogite, in addition to other reasons proposed by predecessors, needs to be considered to explain the high-velocity anomaly of the Farallon plate.

Zoisite is not a predominant mineral in subducting slabs at shallow depths; it mainly comes from the metamorphic reaction of amphibole during subduction. However, this reaction occurs at ~2–3 GPa and 500–700 °C (Poli and Schmidt, 1995). In addition, Usui et al. (2003) also mentioned that the metamorphic conditions of zoisite eclogite xenoliths from the Farallon plate were 560–700 °C at 3 GPa and 600–760 °C at 5 GPa (Poli and Schmidt, 1995; Usui et al., 2003). Moreover, the thermal stability of zoisite varies in different systems; for example, zoisite is stable only up to 3.1 GPa and 650 °C in the basalt + water system (Forneris and Holloway, 2003), while it can be stable at 6.6 GPa and 950 °C in the CaO-Al_2O_3-SiO_2-H_2O system (Poli and Schmidt, 1998; Mao et al., 2007). Furthermore, previous studies using X-ray diffraction (XRD) indicated that the metastability of zoisite reaches up to ~7 GPa and 1000 °C under simultaneous high-temperature and high-pressure conditions (Grevel et al., 2000). In general, previous studies on the stability of zoisite were conducted at relatively low pressures and high temperatures (Pawley et al., 1998; Poli and Schmidt, 1998; Grevel et al., 2000; Forneris and Holloway, 2003; Mao et al., 2007). Additionally, the temperature conditions of previous studies were consistent with the geotherms of hot subduction or normal mantle. However, there are also many cold subducting slabs in the deep Earth (e.g., the Tonga slab and Farallon slab); thus, it is necessary to study the metastability of zoisite under cold subduction conditions (relatively low-temperature and high-pressure conditions) to fully understand the process by which epidote group minerals carry water into the deep Earth (Bina and Navrotsky, 2000; Wang et al., 2013).

An accurate understanding of the thermoelastic properties of zoisite is essential for deriving seismic velocity and density profiles and establishing reliable mineralogical models of subducting slabs. To date, some studies have focused on the pressure-volume (*P-V*) equation of state of zoisite by XRD and theoretical calculations (Holland et al., 1996; Comodi and Zanazzi, 1997; Winkler et al., 2001; Mao et al., 2007; Alvaro et al., 2012; Xu et al., 2019b). However, previous studies have produced significantly different results; for instance, the reported zero-pressure bulk modulus (K_0) of zoisite ranged from 102(7) GPa to 279(9) GPa. Furthermore, only two previous studies have investigated the pressure-volume-temperature (*P-V-T*) equation of state of zoisite (Pawley et al., 1998; Grevel et al., 2000). However, the thermal expansion coefficient ($\alpha_{V} = \alpha_{0V} + \alpha_{1V} \times T$) obtained by Pawley et al. (1998) is 33% larger than that of Grevel et al. (2000), while the temperature derivative of the bulk modulus ($(\partial K/\partial T)_P$) reported by Pawley et al. (1998) is 50% smaller than that reported by Grevel et al. (2000). Therefore, there is still controversy regarding the thermal equation of state for zoisite, which requires further investigation.

In this study, we investigated the thermoelasticity and metastability of a natural zoisite at high pressures (of up to ~24.8 GPa) and relatively low temperatures (of up to 700 K) using an externally heated diamond anvil cell combined with in situ synchrotron single crystal-XRD (SC-XRD). The purpose was to identify the thermoelasticity and thermal stability of zoisite at high pressures and relatively low temperatures. Furthermore, by fitting the present *P-V-T* data to the high-temperature Birch-Murnaghan equation of state (EoS), we obtained the thermal EoS parameters of zoisite. Finally, we modeled the density and bulk sound velocity profiles of zoisite under cold subduction conditions and further discussed the stability of zoisite in cold subduction slabs and the possible cause of high-velocity anomalies in the Farallon plate.

SAMPLE AND EXPERIMENTS

Sample

A natural, colorless, and transparent zoisite sample with good crystal morphology was used in this study. As shown in Table 1, the chemical composition of the zoisite sample was $(Ca_{1.929}Mg_{0.003}Na_{0.002}Ni_{0.001})_{1.934}(Al_{2.972}Cr_{0.002}Mn_{0.002}P_{0.001})_{2.977}Si_{3.065}O_{12}OH$ based on the results of electron microprobe analysis using a JXA-8230 electron microprobe at Chang'An University, Xi'an, China. The analytic acceleration voltage was 15 kV, the beam current was 20 nA, and the beam diameter was 5 μm.

Experiments

A BX90-type externally heated diamond anvil cell (EHDAC) (Kantor et al., 2012), equipped with a pair of 500 μm culet-size diamond anvils, was employed for high temperature and pressure (up to 24.8 GPa and 700 K) SC-XRD experiments. A rhenium plate was preindented to a thickness of ~60 μm, and a hole with a diameter of ~360 μm was drilled onto the indented area to serve as the sample chamber. A gold plate and neon gas were used as the pressure calibration material (Fei et al., 2007) and pressure medium, respectively, which were loaded along with single crystal zoisite into the sample chamber. The size and thickness of single crystal zoisite are ~80 × 85 μm^2 and ~20 μm, respectively.

The high-temperature and high-pressure SC-XRD experiments were performed in the 13-BM-C station, GeoSoilEnviroCARS, of the Advanced Photon Source at Argonne National Laboratory, Lemont, Illinois, USA (Zhang et al., 2017; Xu et al., 2022). The initial pressure after gas loading was ~0.5 GPa. Gold XRD data were collected before and after sample data collection at each *P-T* point, and the pressure varied less than ± 0.1 GPa. Moreover, at each *P-T* condition, the temperature of the sample chamber was actively stabilized within ±1 K using the temperature-voltage feedback loop with a remotely controlled DC power supply and a K-type thermocouple (Huang et al., 2020, 2021).

RESULTS AND DISCUSSION

P-V-T Equation of State for Zoisite

As shown in Table 2, the unit-cell parameters and volumes of zoisite at high pressures and temperatures were refined by APEX3 software (Bruker). Our results show that zoisite has no phase transitions up to 24.8 GPa and 700 K. Additionally, the ambient unit-cell volume

TABLE 1. THE CHEMICAL COMPOSITION OF ZOISITE (WT%)

	1	2	3	4	5	Average
SiO_2	40.25	40.16	41.17	40.25	40.21	40.41 ± 0.38
Al_2O_3	32.81	33.26	33	33.18	33.11	33.07 ± 0.16
FeO	–	0.01	0.01	–	–	0.01 ± 0.003
CaO	23.46	23.61	23.67	23.7	23.72	23.63 ± 0.09
MgO	0.02	0.04	0.03	0.04	0.03	0.03 ± 0.01
Na_2O	–	–	–	–	0.04	0.04
K_2O	–	–	–	–	–	–
TiO_2	–	–	–	–	–	–
MnO	0.05	0.01	–	0.03	0.06	0.04 ± 0.02
NiO	–	0.01	–	0.04	0.05	0.03 ± 0.02
Cr_2O_3	0.01	0.04	–	0.02	0.06	0.03 ± 0.02
P_2O_5	0.07	0.02	0.05	–	–	0.05 ± 0.02
Total	96.67	97.156	97.937	97.251	97.288	97.26 ± 0.41

$(Ca_{1.929}Mg_{0.003}Na_{0.002}Ni_{0.001})_{1.934}(Al_{2.972}Cr_{0.002}Mn_{0.002}P_{0.001})_{2.977}Si_{3.065}O_{12}OH$

Note: Dash indicates below detection limit. Average composition ± standard deviation: 0.01 ± 0.003.

Downloaded from http://pubs.geoscienceworld.org/gsa/gsabulletin/article-pdf/135/5-6/1178/5827011/b36479.1.pdf
by Argonne National Laboratory user

TABLE 2. THE UNIT-CELL PARAMETERS AND VOLUME OF ZOISITE AT HIGH PRESSURES AND HIGH TEMPERATURES

Pressure (GPa)	Temperature (K)	*a* (Å)	*b* (Å)	*c* (Å)	*V* (Å^3)
0	300	16.2002 (2)	5.5465 (1)	10.0303 (2)	901.26 (3)
0.60 (1)	300	16.1820 (9)	5.5400 (5)	10.0150 (7)	897.83 (8)
1.70 (3)	300	16.1598 (9)	5.5224 (4)	9.9764 (6)	890.31 (7)
2.33 (2)	350	16.1479(9)	5.5169(4)	9.9639(6)	887.65(7)
4.81(4)	350	16.0866(9)	5.4816(3)	9.8894(5)	872.04(5)
5.270(5)	350	16.0792(10)	5.4765(3)	9.8768(6)	869.73(6)
5.85(1)	350	16.0660(9)	5.4694(3)	9.8613(5)	866.54(5)
6.81(2)	350	16.048(1)	5.4609(3)	9.8408(5)	862.42(6)
8.72(2)	350	16.0072(8)	5.4378(6)	9.7904(7)	852.19(9)
9.36(2)	350	15.9944(7)	5.4298(6)	9.7749(6)	848.92(9)
10.88(2)	350	15.941(1)	5.4125(3)	9.7410(6)	840.46(6)
11.83(1)	350	15.919(2)	5.4040(4)	9.7125(8)	835.5(8)
13.00(9)	350	15.892(1)	5.3901(3)	9.6976(6)	830.69(6)
14.09(2)	350	15.867(2)	5.3808(3)	9.6780(8)	826.3(8)
15.56(5)	350	15.833(3)	5.3705(6)	9.647(1)	820.3(1)
16.66(2)	350	15.8226(6)	5.3634(6)	9.6112(6)	815.63(8)
19.55(5)	350	15.737(4)	5.3332(8)	9.588(2)	804.7(2)
20.23(1)	350	15.728(3)	5.3285(6)	9.565(1)	801.6(1)
23.10(6)	350	15.667(3)	5.3046(7)	9.525(2)	791.6(2)
4.453(4)	500	16.108(1)	5.4972(4)	9.9182(7)	878.21(7)
5.69(8)	500	16.080(1)	5.4801(3)	9.8835(6)	870.92(6)
6.07(7)	500	16.0779(7)	5.4787(5)	9.8761(4)	869.95(7)
6.74(9)	500	16.058(1)	5.4673(3)	9.8531(5)	865.04(6)
8.27(7)	500	16.0315(7)	5.4529(6)	9.8189(5)	858.35(9)
9.50(16)	500	15.996(1)	5.4361(3)	9.7880(6)	851.14(6)
10.5(1)	500	15.9841(7)	5.4265(6)	9.7704(6)	847.47(8)
11.7(1)	500	15.9546(6)	5.4126(5)	9.7357(5)	840.74(8)
12.7(1)	500	15.9387(7)	5.4035(6)	9.7199(6)	837.13(9)
13.9(2)	500	15.889(1)	5.3883(3)	9.6902(6)	829.6(6)
15.1(1)	500	15.8860(7)	5.3800(6)	9.6700(6)	826.46(9)
16.5(2)	500	15.832(3)	5.3680(5)	9.642(1)	819.4(1)
18.6(1)	500	15.8053(7)	5.3488(6)	9.6018(6)	811.74(9)
20.3(2)	500	15.7653(8)	5.3298(7)	9.5643(7)	803.66(1)
21.7(1)	500	15.719(4)	5.3232(9)	9.564(2)	800.3(2)
24.0(2)	500	15.665(3)	5.3046(7)	9.516(2)	790.7(2)
6.8(1)	700	16.0757(9)	5.4819(5)	9.8842(5)	871.05(8)
8.0(1)	700	16.0535(7)	5.4683(5)	9.8527(5)	864.91(8)
11.3(1)	700	15.9836(7)	5.4298(5)	9.7711(6)	848.02(8)
13.59(3)	700	15.9327(7)	5.4039(6)	9.7179(6)	836.7(9)
15.0(2)	700	15.9047(7)	5.3911(6)	9.6921(6)	831.05(9)
17.4(2)	700	15.8552(7)	5.3678(6)	9.6470(6)	821.04(9)
21.5(3)	700	15.7708(7)	5.3344(7)	9.5736(7)	805.4(9)
24.8(1)	700	15.678(2)	5.3051(4)	9.516(1)	791.4(1)

Note: The numbers in parentheses represent one standard deviation.

($V_{T0} = 901.26(3)$ Å^3) of zoisite was obtained in this study, which is consistent with previous studies (Comodi and Zanazzi, 1997; Pawley et al., 1998; Grevel et al., 2000; Alvaro et al., 2012; Xu et al., 2019b). Furthermore, the *P-V-T* data (Table 2) were fitted to the high-temperature Birch-Murnaghan equation of state (BM-EoS) using EoSfit7c (Angel et al., 2014) to obtain the thermal EoS parameters, including the zero-pressure bulk modulus (K_0), thermal expansion coefficient (α_V), and the temperature derivative of K_0 ($(\partial K_T/\partial T)_P$) (Fig. 1 and Table 3). By fixing the pressure derivative of the bulk modulus ($K'_0 = 4$), we obtained $K_0 = 134.7(8)$ GPa, $(\partial K/\partial T)_P = -0.011(4)$ GPa/K, $\alpha_{0V} = 1.9(7)$ 10^{-5} K^{-1}, and $\alpha_{1V} = 3(2) \times 10^{-8}$ K^{-2}.

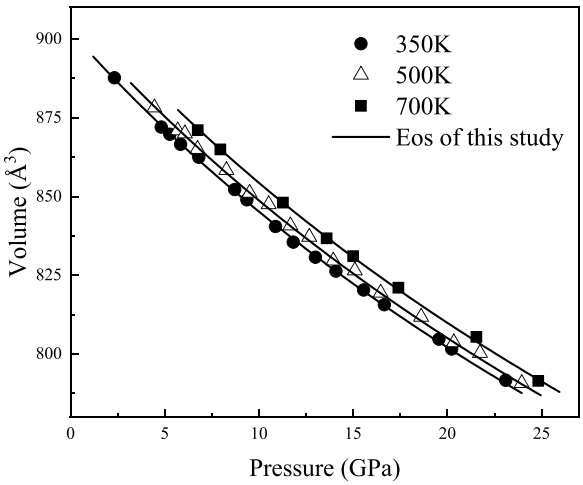

Figure 1. *P-V-T* data for zoisite in this study are plotted. Isothermal compression curves at various temperatures are represented by solid lines from the high-temperature BM EoS at 350 K, 500 K, and 700 K. The error bars of the data points are smaller than the symbols.

To date, the bulk modulus and its pressure derivative of zoisite have been investigated extensively with various experimental techniques (Table 3). However, there are still discrepancies in the K_0 values (from 102(7) GPa to 279(9) GPa). We infer that there are three possible reasons for the difference in K_0 of zoisite reported by previous studies, namely, the different pressure media, the different mineral compositions, and K'_0. First, Holland et al. (1996) measured the compressibility of zoisite at high pressures of up to 13.79 GPa using the energy dispersive-XRD (ED-XRD) method with a methanol:ethanol = 4:1 pressure medium and obtained an abnormally high value of $K_0 = 279(9)$ GPa (fixed $K'_0 = 4$). The experimental pressure range (~13.79 GPa) of Holland et al. (1996) exceeded the hydrostatic pressure limit (~10 GPa) of methanol:ethanol = 4:1 (Angel et al., 2007; Klotz et al., 2009); thus, the $K_0 = 279(9)$ GPa obtained by Holland et al. (1996) could be overestimated in comparison with those obtained by high-pressure XRD conducted in quasihydrostatic pressure conditions. In addition, in static compression studies, there is a trade-off between the fitted K_0 and K'_0, which have a negative correlation (Gatta et al., 2011). With fixed $K'_0 = 4$, the K_0 values of zoisite obtained by Pawley et al. (1998) and Grevel et al. (2000) are 125 (3) GPa and 125 (2) GPa, respectively. To exclude the possible influence of K'_0 on the fitted K_0, we fixed $K'_0 = 4$ and refitted the XRD experimental data obtained by Comodi and Zanazzi (1997), Alvaro et al. (2012), and Xu et al. (2019b). The refitted K_0 values of Comodi and Zanazzi (1997), Alvaro et al. (2012), and Xu et al. (2019b) were 104 (3) GPa, 131.6 (8) GPa, and 137 (2) GPa for zoisite with 10 mol%, 12 mol%, and 11 mol% ferric end-member ($Ca_2Al_2Fe^{3+}Si_3O_{12}(OH)$), respectively. In summary, the K_0 of zoisite obtained in previous studies was in the range of 104–137 GPa when K'_0 was fixed to 4. In addition, the mineral composition may affect K_0 when K'_0 is fixed to 4. For example, Comodi and Zanazzi (1997) obtained $K_0 = 104$ (3) GPa for zoisite containing ~10 mol% ferric end-member, which is 16.8% lower than the $K_0 = 125$ (3) GPa obtained by Pawley et al. (1998) for zoisite containing ~3 mol% ferric end-member. However, the $K_0 = 134.7(8)$ GPa of zoisite with no ferric end-member obtained in this study is 22.8%, 7.2%, 7.2%, and 8.4% higher than the results of Comodi and Zanazzi (1997), Pawley et al. (1998), Grevel et al. (2000), and Mao et al. (2007), respectively, but is close to the results of Alvaro et al. (2012) and Xu et al. (2019b) for zoisite with 12 mol% and 11 mol% ferric end-member, respectively. A comparison of our results with those of previous studies on zoisite

Downloaded from http://pubs.geoscienceworld.org/gsa/gsabulletin/article-pdf/135/5-6/1178/5827011/b36479.1.pdf
by Argonne National Laboratory user

TABLE 3. THERMAL EOS PARAMETERS OF ZOISITE

Composition	P(GPa)	T(K)	Method	K_0(GPa)	K'_0	V_0 (Å^3)	Pressure medium	α_{0V} (10^{-5} K^{-1})	α_{1V} (10^{-8} K^{-2})	$(\partial K/\partial T)_P$ (GPa/K)	Reference
$Ca_2Al_2(Al_{0.9}Fe_{0.1})Si_3O_{12}OH$	5	300	SC-XRD	102(7)	4.8(4)	903.6(4)	methanol: ethane: water =16: 3: 1	–	–	–	Comodi and Zanazzi (1997)
$Ca_{1.99}Sr_{0.01})(Al_{2.99}V_{0.01})Si_3O_{12}OH$	7.76	300	SC-XRD	122.1(7)	6.8(2)	903.39(5)	methanol: ethane = 4:1	–	–	–	Alvaro et al. (2012)
$(Ca_{1.99}Sr_{0.01})(Al_{2.88}Fe_{0.12})Si_3O_{12}OH)$	7.63	300	SC-XRD	119.1(7)	7.3(2)	906.95(5)	methanol: ethane = 4:1	–	–	–	Alvaro et al. (2012)
$Ca_{1.99}(Al_{2.87}Fe_{0.11})Si_{3.00}O_{12}OH$	34	300	SC-XRD	118(1)	6.3(2)	904.77(8)	Ne	–	–	–	Xu et al. (2019b)
$Ca_2Al_{2.97\pm0.01}Fe_{0.03\pm0.01}Si_3O_{12}(OH)$	6.1	1073	ED-XRD	125(3)	4(fixed)	907(1)	NaCl	3.86	0(fixed)	–0.0296(6)	Pawley et al. (1998)
$Ca_2Al_3(SiO_4)(Si_2O_7)O(OH)$	7	1273	ED-XRD	125(2)	4(fixed)	901.0(6)	Vaseline	3.1(4)	–0.6(6)	0.0156(6)	Grevel et al. (2000)
$Ca_2Al_3(SiO_4)(Si_2O_7)O(OH)$	7	1273	ED-XRD	125(2)	4(fixed)	901.0(6)	Vaseline	2.6(1)	0(fixed)	0.0148(6)	Grevel et al. (2000)
$Ca_2Al_3Si_3O_{12}(OH)$	13.79	300	ED-XRD	279(9)	4(fixed)	904.4(8)	methanol: ethane = 4:1	6.77	–	–	Holland et al. (1996)
$Ca_2Al_3Si_3O_{12}(OH)$	0	300	BS	123.4(4)	4(fixed)	–	–	–	–	–	Mao et al. (2007)
$Ca_2Al_3[O][OH]Si_2O_7[SiO_4]$	0	300	DFT	117(2)	–	900	–	–	–	–	Winkler et al. (2001)
$(Ca_{1.929}Mg_{0.003}Na_{0.002}Ni_{0.001})_{1.934}(Al_{2.972}Cr_{0.002}Mn_{0.002}P_{0.001})_{2.977}Si_{3.065}O_{12}OH$	24.8	700	SC-XRD	134.7(8)	4(fixed)	901.26(3)	Ne	1.9(7)	3(2)	–0.011(4)	This study
$(Ca_{1.929}Mg_{0.003}Na_{0.002}Ni_{0.001})_{1.934}(Al_{2.972}Cr_{0.002}Mn_{0.002}P_{0.001})_{2.977}Si_{3.065}O_{12}OH$	24.8	700	SC-XRD	134.6(4)	4(fixed)	901.26(3)	Ne	3.25(4)	0(fixed)	–0.0108(6)	This study

Note: Dash indicates no data; ED-XRD—energy dispersive–X-ray diffraction; DFT—density functional theory; SC-XRD—single crystal–X-ray diffraction; BS—Brillouin scattering.

shows no linear correlation between the ferric end-member and bulk modulus. In general, the results of K_0 obtained from this study may objectively reflect the compressional properties of zoisite.

To date, much of the controversy from previous studies about the α_V and $(\partial K_T/\partial T)_P$ of zoisite remains (Holland et al., 1996; Pawley et al., 1996; Pawley et al., 1998; Grevel et al., 2000). The α_V and $(\partial K_T/\partial T)_P$ obtained in this study are 3.25 (4) 10^{-5} K^{-1} and –0.011 (4) GPa/K, respectively. Pawley et al. (1998) obtained $\alpha_V = 3.86 \times 10^{-5}$ K^{-1} and $(\partial K_T/\partial T)_P = -0.0296(6)$ GPa/K using ED-XRD methods under high P-T conditions of up to 6.1 GPa and 1073 K. The α_V and $(\partial K_T/\partial T)_P$ obtained for zoisite by Pawley et al. (1998) are 15.8% higher and 62.8% lower than the results of this study, respectively. We infer that the main reason for the differences in α_V and $(\partial K_T/\partial T)_P$ values of these two studies are the different mineral compositions. The zoisite sample in Pawley et al. (1998) contains ~3 mol% ferric end-member, but our zoisite sample is nearly Fe-free. However, using the same method at high P-T conditions of up to 7 GPa and 1273 K, Grevel et al. (2000) obtained $\alpha_V = 2.6$ (1) 10^{-5} K^{-1} and $(\partial K_T/\partial T)_P = 0.0148$ (6) GPa/K for Fe-free zoisite. A positive $(\partial K_T/\partial T)_P$ of zoisite obtained by Grevel et al. (2000), as suggested by the authors themselves, does not make sense. Grevel et al. (2000) possibly obtained inaccurate thermal EoS parameters of zoisite because the few high-pressure points (only three points) under each isothermal temperature curve are available. Therefore, Grevel et al. (2000) obtained the values of $\alpha_V = 3.4$ (5) $\times 10^{-5}$ K^{-1} and $(\partial K_T/\partial T)_P = -0.0128$ (4) GPa/K by fitting their data together with the data of Pawley et al. (1996) to the high-temperature BM EoS. Thus, we believe that the α_V (3.25 (4) $\times 10^{-5}$ K^{-1}) and $(\partial K_T/\partial T)_P$ (–0.011(4) GPa/K) obtained for zoisite in this study are reliable.

P-T Stability of Zoisite

The distribution and cycling of water in the deep Earth is vital to our understanding of the dynamic processes in the deep Earth (Zheng and Hermann, 2014; Zheng et al., 2016). Hydrous minerals are considered to be the main carriers of water into the deep Earth. Many studies have discussed the strong relationship between the subduction depth of hydrous minerals and the depth of water release in subduction zones (e.g., Zheng and Hermann, 2014; Zheng et al., 2016; Zheng, 2019). On the other hand, the geothermal gradient strongly affects the depth at which hydrous minerals dehydrate in subducting slabs and thus affects water transport in the deep Earth.

Under normal geothermal gradient conditions, many hydrous minerals in the shallow crust or upper mantle depth range are not stable (Lempart et al., 2020). However, the dehydration of hydrous minerals is likely to be inhibited by low temperatures in cold subduction, especially super cold subduction, and hydrous minerals will be subducted into the deep mantle along the subduction plate and carry a large amount of water into the middle and lower parts of the upper mantle. Thus, hydrous minerals subducted to deep Earth under cold subduction will exert a profound influence on geological processes in the deep Earth (Chen et al., 2020; Thompson et al., 2020).

Zoisite is a typical hydrous mineral in subducted plates and contains ~2 wt% water (Forneris and Holloway, 2003; Mao et al., 2007). Several studies have investigated the high P-T stability of zoisite (e.g., Delany and Helgeson, 1978; Schmidt and Poli, 1994; Comodi and Zanazzi, 1997; Pawley et al., 1998; Poli and Schmidt, 1998; Grevel et al., 2000; Alvaro et al., 2012; Xu et al., 2019b). Figure 2 shows the stability area and metastable area of zoisite under high P-T conditions. The stability area was mainly obtained from the phase equilibrium experiments of Delany and Helgeson (1978), Schmidt and Poli (1994), and Poli and Schmidt (1998), and the metastable area was mainly obtained from the XRD experiments of Comodi and Zanazzi (1997), Pawley et al. (1998), Grevel et al. (2000), Alvaro et al. (2012), Xu et al. (2019b), and this study.

Under normal geothermal gradient conditions, zoisite breaks down into grossular + lawsonite + kyanite + coesite (G + L+K + C) at depths of ~53–215 km (1.6 GPa–6.5 GPa, 813 K–1253 K) or breaks down into grossular + kyanite + coesite + H_2O at depths of >248 km (7.5 GPa and 1293 K) (Newton and Kennedy, 1963; Delany and Helgeson, 1978; Holland and Powell, 1990; Schmidt and Poli, 1994). In hot subduction zones, such as the Aleutian subduction zone, zoisite breaks down into a G + L+K + C assemblage at 165 km (5 GPa

Downloaded from http://pubs.geoscienceworld.org/gsa/gsabulletin/article-pdf/135/5-6/1178/5827011/b36479.1.pdf
by Argonne National Laboratory user

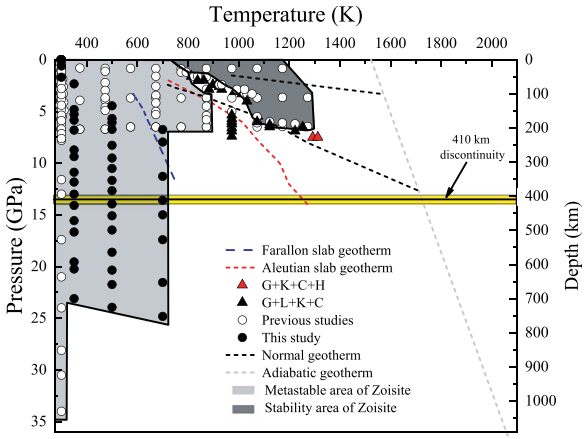

Figure 2. *P-T* stability of zoisite is plotted. The black solid circles represent the data points of this experiment, and the white hollow circles represent the data points of previous studies (Delany and Helgeson, 1978; Comodi and Zanazzi, 1997; Pawley et al., 1998; Poli and Schmidt, 1998; Grevel et al., 2000; Winkler et al., 2001; Alvaro et al., 2012; Xu et al., 2019b). The dark gray area represents the stability area of zoisite. The light gray area represents the metastable area of zoisite. Black solid triangles represent the stability of grossular + lawsonite + kyanite + coesite (G + L+K + C), and red solid triangles represent the stability of grossular + kyanite + coesite + H_2O (G+ K + C+H). The blue dotted line represents the geothermal gradient of the Farallon plate, and the red dotted line represents the geothermal gradient of the Aleutian plate. The black dotted lines represent the normal geotherm. The gray dotted line represents the adiabatic geotherm.

and 973 K) (Poli and Schmidt, 1998). However, the stable depth of zoisite is quite different in cold or super cold subduction zones, e.g., the Farallon subduction zone, where zoisite can be metastable up to 215 km deep (6.5 GPa and 500 K; Pawley et al., 1998; Grevel et al., 2000). Furthermore, this study also indicates that zoisite does not undergo phase transition or dehydration at 24.8 GPa and 700 K; thus, combined with the results of previous studies, we conclude that the zoisite can be metastable to a depth of ~300 km under cold subduction conditions (temperature gradient <5 K/km; Fig. 3).

IMPLICATIONS

There are many ultrahigh/high-pressure metamorphic zones around the world (e.g., Dabie-Sulu and Tibet; Li et al., 2004). According to the statistics, zoisite is a typical secondary mineral in ultrahigh/high-pressure eclogite (for example, Dabie-Sulu and Tibet ultrahigh/high-pressure metamorphic zone). In addition, the mineral content of zoisite in eclogite is usually ~7 vol% in the Dabie-Sulu ultrahigh/high-pressure metamorphic zone (e.g., Zheng et al., 2007; Zhang et al., 2008; Liu et al., 2009, 2010; Zheng et al., 2011; Chen et al., 2014; Li et al., 2018; Feng et al., 2021) and ~10 vol% in the Tibet ultrahigh/high-pressure metamorphic zones (e.g., Li et al., 2009; Wei et al., 2009; Zheng, 2009; Xiao et al., 2012; Cheng et al., 2015; Dong et al., 2016; Zhang et al., 2016, 2019). More importantly, among the major ultrahigh/high-pressure metamorphic zones around the world, the Farallon plate is also an important ultrahigh-pressure metamorphic zone that contains a high amount of zoisite. We have summarized the mineral proportions of zoisite in eclogite of the Farallon plate, and the average is ~16.0 vol% and the maximum is ~41.4 vol% (e.g., Selverstone et al., 1999; Hacker and Abers, 2004; Zack et al., 2004; Usui et al., 2003, 2006, 2007; Marot et al., 2014; Hernández-Uribe and Palin, 2019; Bustamante et al., 2021). Thus, zoisite is a key component of eclogite in the Farallon plate.

The Subducted Depth of Zoisite Eclogite in the Farallon Plate

The density profile of zoisite was modeled using its thermal EoS parameters (Table 4) and then compared with other typical hydrous minerals (e.g., diaspore, epidote, lawsonite, and antigorite), eclogite, harzburgite, and the PREM/AK135 model (Fig. 3; Kennett et al., 1995; Ballaran and Angel, 2003; Nishihara et al., 2003; Yang et al., 2014; Xu et al., 2019a; Ye et al., 2021). As illustrated in Figure 3, the densities of all hydrous minerals increase gradually with depths from 100 km to 400 km along the cold subduction slabs. The density of zoisite is ~3.1% and ~0.5% lower than those of epidote and diaspore, respectively, but is ~8.3% and ~28.9% higher than those of lawsonite and antigorite, respectively, at 100 km depth. Moreover, at the depth of 400 km, the density of zoisite is ~3.2% and ~0.6% lower than those of epidote and diaspore, respectively, but is ~7.8% and ~23.7% higher than those of lawsonite and antigorite, respectively. Moreover, the density of zoisite is also ~1.1% and ~1.0% higher than the PREM and AK135 models at depths of 100–400 km, respectively.

To assess the density relationship between zoisite eclogite and the PREM model, we also modeled the density profile of representative zoisite eclogite in the Farallon plate (23.0 vol% garnet + 61.0 vol% omphacite + 16.0 vol% zoisite), which is shown in Table 5. The density profiles of this representative zoisite eclogite were calculated using the reported thermal EoS

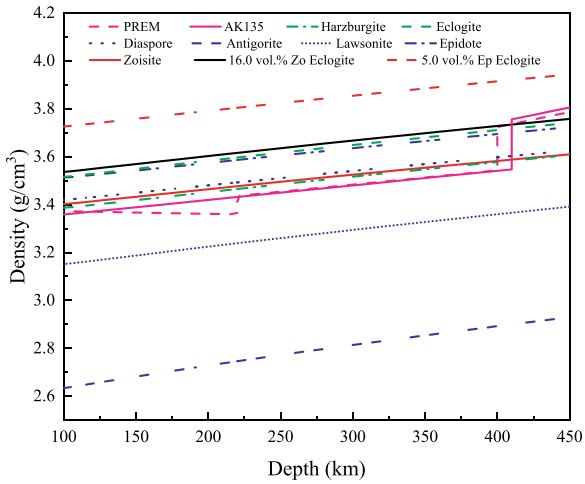

Figure 3. Modeled density profiles of zoisite and other hydrous minerals are plotted—Lawsonite (Ballaran and Angel, 2003), Antigorite (Yang et al., 2014), Diaspore (Huang et al., 2021), and Epidote (Li et al., 2021)—to ~450 km along the Farallon slab geotherm. They are compared with those of the PREM and AK135 models (Dziewonski and Anderson, 1981; Kennett et al., 1995). The densities along the Farallon slab geotherm are shown for the epidote eclogite with 5.0 vol% epidote (49.0 vol% garnet + 46.0 vol% omphacite + 5.0 vol% epidote), the harzburgite (74.0 vol% olivine + 21.0 vol% orthopyroxene + 3.0 vol% omphacite + 2.0 vol% spinel), the eclogite (21.0 vol% garnet + 79.0 vol% omphacite), and the zoisite eclogite xenoliths with 16 vol% zoisite (61.0 vol% omphacite + 23.0 vol% garnet + 16.0 vol% zoisite) found in the Colorado Plateau. Thermal EoS parameters for density models are shown in Table 4 (Ballaran and Angel, 2003; Nishihara et al., 2003; Yang et al., 2014; Li et al., 2021; Ye et al., 2021).

Downloaded from http://pubs.geoscienceworld.org/gsa/gsabulletin/article-pdf/135/5-6/1178/5827011/b36479.1.pdf
by Argonne National Laboratory user

TABLE 4. THERMAL EOS PARAMETERS OF RELEVANT MINERALS USED FOR DENSITY MODELS

Mineral	V_0 (Å^3)	K_0(GPa)	K'_0	α_{0V} (10^{-5} K^{-1})	α_{1V} (10^{-8} K^{-2})	$(\partial K/\partial T)_P$ (GPa/K)	Reference
Zoisite $(Ca_{1.929}Mg_{0.003}Na_{0.002}Ni_{0.001})_{1.934}(Al_{2.972}Cr_{0.002}Mn_{0.002}P_{0.001})_{2.977}Si_{3.065}O_{12}OH$	901.26(3)	134.7(8)	4(fixed)	1.9(7)	3(2)	–0.011(4)	This study
Epidote $Ca_{1.97}Al_{2.15}Fe_{0.84}(SiO_4)(Si_2O_7)O(OH)$	456.2(2)	133.2(6)	4(fixed)	4.3(2)	0(fixed)	–0.022(5)	Li et al. (2021)
Lawsonite $CaAl_2Si_2O_7(OH)_2.H_2O$	674.5(6)	106(4)	5(2)	3.7(3)	0(fixed)	–0.020(7)	Grevel et al. (2000)
Antigorite $(Mg_{2.64}Fe_{0.1}Al_{0.17}Cr_{0.02})Si_{2.05}O_5(OH)_4$	367.3(2)	62.9	6.1(fixed)	3.9(5)	0(fixed)	–0.027(4)	Yang et al. (2014)
Olivine $(Mg_{0.909}Fe_{0.089}Mn_{0.001}Ni_{0.004})_{2.006}Si_{0.995}O_4$	291.7(1)	126(3)	3.9(3)	4.7(7)	0(fixed)	–0.02(1)	Ye et al. (2021)
Orthopyroxene $(Mg_{0.868}Fe_{0.079}Ca_{0.023}Al_{0.013}Cr_{0.007}Na_{0.003}Mn_{0.002}Ti_{0.006})_{2.000}(Si_{0.969}Al_{0.031})_2O_6$	834.8(5)	116(3)	7(1)	5.4(5)	0(fixed)	–0.05(1)	Ye et al. (2021)
Spinel $(Mg_{0.743}Fe_{0.269}Ni_{0.004}Ti_{0.006}Mn_{0.005}Na_{0.001})_{1.028}(Al_{0.604}Cr_{0.358}Fe_{0.037}Si_{0.001})_2O_4$	539.4(3)	196(2)	3.4(4)	2.8(2)	0(fixed)	–0.020(8)	Ye et al. (2021)
Garnet $(Mg_{0.144}Fe_{0.618}Ca_{0.219}Mn_{0.021})_{3.006}(Al_{0.947}Fe_{0.034}Si_{0.012})_{1.986}Si_{3.000}O_{12}$	1564.9 (1)	159(1)	5.0(2)	1.7(2)	2.9(5)	–0.010(4)	Xu et al. (2019a)
Omphacite $(Di_{63}Jd_{37})$	423.8	126(1)	4(fixed)	2.2(1)	0(fixed)	–0.015(4)	Nishihara et al. (2003)
Diaspore $(Al_{1.002}Fe_{0.003}OOH)$	118.15(4)	143(1)	4(fixed)	2.7(2)	0(fixed)	–0.017	Huang et al. (2021)

parameters of garnet, omphacite, and zoisite determined by previous studies and this study (Table 4). As shown in Figure 3, the density of these representative zoisite eclogite xenoliths is ~5.1% and ~5.3% greater than the densities of PREM at 100 km and 400 km, respectively. Thus, combined with the metastable depth of zoisite obtained in this study, we infer that the zoisite eclogite could subduct to at least ~300 km depth.

Zoisite Eclogite and the High-Velocity Anomalies in the Farallon Plate

The major hydrous minerals in subduction zones include diaspore, lawsonite, epidote, zoisite, and antigorite (Jiang et al., 2008), etc. Therefore, we calculated their bulk sound velocity at depths from 100 km to 450 km using the reported thermal EoS parameters along the Farallon plate geotherm (Fig. 4; Suzuki and Anderson, 1983; Hofmeister and Mao, 2002; Hacker et al., 2003; Huang et al., 2021; Li et al., 2021). The bulk sound velocity (V_b) of minerals and rocks can be calculated using the following equations:

$$K_S = (1+\alpha\gamma T)K_T \quad (1)$$

$$V_b = \sqrt{K_S/\rho} \quad (2)$$

where K_T is the isothermal bulk modulus, K_S is the adiabatic bulk modulus, ρ is the density, γ is the thermodynamic Grüneisen parameter, α is the thermal expansion coefficient, V_b is the bulk sound velocity, and T is the temperature. The K_T of minerals and rocks can be calculated using the following equations:

$$K_T = K_0 + \left(\left(\frac{\partial K}{\partial T}\right)_P\right)\times(T-300) + \left(\left(\frac{\partial K}{\partial P}\right)_T\right)\times P \quad (3)$$

where K_T is the isothermal bulk modulus at a certain temperature and pressure, K_0 is the isothermal bulk modulus under ambient conditions, $\left(\frac{\partial K}{\partial T}\right)_P$ is the temperature derivative of K under constant pressure, $\left(\frac{\partial K}{\partial P}\right)_T$ is the pressure derivative of K under constant temperature, and P is pressure. The calculation of Ks for rocks using the Voight–Ruess–Hill (VRH) averaging method can be represented as follows.

$$\text{Voight(V)}: Ks = \sum_{i=1}^{N} K_i \times V_i \quad (4)$$

$$\text{Ruess(R)}: K_S^{-1} = \sum_{i=1}^{N} K_S^{-1} \times V_i \quad (5)$$

$$\text{VRH}: K_{VRH} = (K_V + K_R)/2 \quad (6)$$

where N is the number of mineral species, K_i represents K_T for the ith mineral, V_i represents the percentage of the ith mineral volume in the rock, and K_V and K_R represent the calculated result of Ks by the Voight and Ruess methods, respectively.

TABLE 5. MINERAL PROPORTIONS OF ECLOGITE

	5.0 vol% Ep eclogite	Eclogite	16.0 vol% Zo eclogite
Garnet (vol%)	49.0	21.0	23.0
Omphacite (vol%)	46.0	79.0	61.0
Epidote/zoisite (vol%)	5.0	—	16.0

Note: Dash indicates epidote- and zoisite-free.

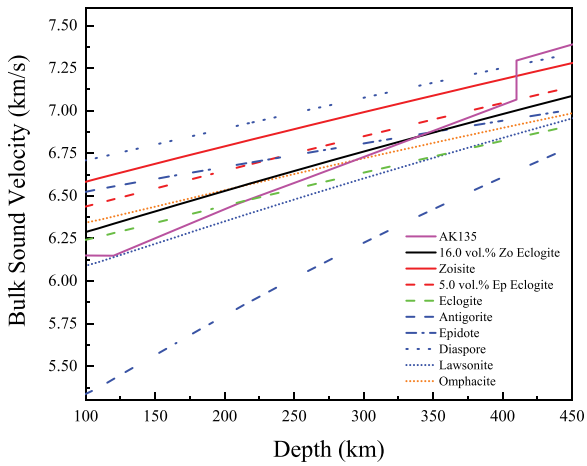

Figure 4. Bulk sound velocities are plotted for zoisite, epidote, antigorite, diaspore, lawsonite, omphacite, 5.0 vol% Ep eclogite (49.0 vol% garnet + 46.0 vol% omphacite + 5.0 vol% epidote), the eclogite (21.0 vol% garnet + 79.0 vol% omphacite), and 16.0 vol% Zo eclogite (61.0 vol% omphacite + 23.0 vol% garnet + 16.0 vol% zoisite). The mineral composition is shown in Table 5. The bulk sound velocity profile of the AK135 seismic model is also plotted for comparison.

As shown in Figure 4, the bulk sound velocity of zoisite is ~2.0% lower than that of diaspore but is ~0.8%, ~25.5%, ~7.7%, and ~3.5% higher than those of epidote, antigorite, lawsonite, and omphacite at 100 km depth, respectively. In addition, at 300 km depth, the bulk sound velocity of zoisite is ~1.2% lower than that of diaspore but is ~2.7%, ~12.3%, 5.9%, and ~4.0% higher than those of epidote, antigorite, lawsonite, and omphacite, respectively. In conclusion, zoisite is a high-velocity mineral among the major hydrous minerals in subduction zones at depths of 100–300 km.

Recently, many studies have focused on the causes of the abnormal velocity in the Farallon plate (Van der Lee and Nolet, 1997; Levander

Downloaded from http://pubs.geoscienceworld.org/gsa/gsabulletin/article-pdf/135/5-6/1178/5827011/b36479.1.pdf
by Argonne National Laboratory user

TABLE 6. THERMOELASTIC PROPERTIES OF ZOISITE AND OTHER MINERALS USED FOR ADIABATIC BULK MODULUS (K_S) CALCULATIONS

Mineral composition	K_0(GPa)	K'_0	α_{0V} (10^{-5} K^{-1})	α_{1V} (10^{-8} K^{-2})	y	$(\partial K/\partial T)_P$ (GPa/K)	Reference
Zoisite $(Ca_{1.929}Mg_{0.003}Na_{0.002}Ni_{0.001})_{1.934}(Al_{2.972}Cr_{0.002}Mn_{0.002}P_{0.001})_{2.977}Si_{3.065}O_{12}OH$	134.7(8)	4(fixed)	1.9(7)	3(2)	1.2	–0.011(4)	This study; Hacker et al. (2003)
Olivine $(Mg_{0.893}Fe_{0.100}Mn_{0.001}Ni_{0.004})_{1.996}Si_{0.999}O_4$	126(3)	3.9(3)	4.7(7)	0(fixed)	1.22	–0.02(1)	Ye et al. (2021); Hofmeister and Mao (2002)
Garnet $(Mg_{0.144}Fe_{0.618}Ca_{0.219}Mn_{0.021})_{3.006}(Al_{0.947}Fe_{0.034}Si_{0.012})_{1.986}Si_{3.000}O_{12}$	159(1)	5.0(2)	1.7(2)	2.9(5)	1.202	–0.010(4)	Xu et al. (2019a); Suzuki and Anderson (1983)
Antigorite $(Mg_{2.64}Fe_{0.1}Al_{0.17}Cr_{0.02})Si_{2.05}O_5(OH)_4$	62.9	6.1(fixed)	3.9(5)	0(fixed)	0.5	–0.027(4)	Yang et al. (2014); Hacker et al. (2003)
Omphacite $(Di_{63}Jd_{37})$	126(1)	4(fixed)	2.2(1)	0(fixed)	0.70	–0.015(4)	Nishihara et al. (2003)
Epidote $Ca_{1.97}Al_{2.15}Fe_{0.84}(SiO_4)(Si_2O_7)O(OH)$	138(2)	3.0(3)	3.8(5)	0(fixed)	1.1	–0.004(1)	Li et al. (2021); Hacker et al. (2003)
Diaspore $(Al_{1.002}Fe_{0.003}OOH)$	143(1)	4(fixed)	2.7(2)	0(fixed)	1.44	–0.017	Huang et al. (2021); Jiang et al. (2008)
Lawsonite $CaAl_2Si_2O_7(OH)_2.H_2O$	106(4)	5(2)	3.7(3)	0(fixed)	0.9	–0.020(7)	Ballaran and Angel (2003); Grevel et al. (2000)

et al., 2011; Sigloch, 2011; Pavlis et al., 2012; Wang et al., 2013). However, previous explanations are still being debated (Van der Lee and Nolet, 1997; Levander et al., 2011; Pavlis et al., 2012; Wang et al., 2013). On the one hand, Levander et al. (2011) argued that the dip angle of the plate caused the positive velocity anomalies. On the other hand, Van der Lee and Nolet (1997) proposed that the temperature anomalies of the Farallon plate could produce positive velocity anomalies and further estimated that every 100 °C decrease in temperature results in an increase of ~1% in the shear wave velocity. Alternatively, Pavlis et al. (2012) reported that the structure of the tectonic plate may cause positive velocity anomalies. Recently, Wang et al. (2013) found that the positive velocity anomalies in the Farallon plate are related to the distribution of high-Mg andesites derived from partial melting of the subducted oceanic crust.

Previous studies have indicated that zoisite eclogite is a key component in the Farallon plate (e.g., Usui et al., 2003, 2006, 2007). Therefore, the presence of zoisite eclogite could be considered to explain the high-velocity anomalies in the Farallon plate. To test this hypothesis, we calculated the bulk sound velocity profiles of representative zoisite eclogite along the Farallon slab geotherm. According to the mineral proportions of representative zoisite eclogite in the Farallon plate, our zoisite eclogite model contains ~61.0 vol% omphacite, ~23.0 vol% garnet, and ~16.0 vol% zoisite (Table 5). The thermal EoS parameters of minerals used in our calculation are listed in Table 6. Moreover, the modeled bulk sound velocity profiles of zoisite eclogite are further compared with the AK135 seismic model (Fig. 4; Kennett et al., 1995). Our results show that the bulk sound velocities of 16.0 vol% zoisite eclogite are ~0.5%–3.0% higher than the AK135 model at 100–300 km depths. The velocity differences are consistent with the seismic observations of the high-velocity anomaly at 100–300 km depths in the Farallon plate (Fig. 5).

Furthermore, to assess whether the presence of zoisite in eclogite is necessary to explain the high-velocity anomaly of the Farallon plate at 100–300 km depths, we also calculated the bulk sound velocity of zoisite- and epidote-free eclogite model (only omphacite and garnet) and epidote eclogite model with 5.0 vol% epidote for comparison (Fig. 4). The zoisite- and epidote-free eclogite model contains ~79.0 vol% omphacite and ~21.0 vol% garnet, which is based on the experimental petrology study (Nishi et al., 2009). The epidote eclogite model contains ~46.0 vol% omphacite, ~49.0 vol% garnet, and ~5.0 vol% epidote, which are summarized from the previous studies of mineral proportions of eclogites in ultrahigh/high-pressure metamorphic zones. As shown in Figure 4, the velocity difference between the zoisite- and epidote-free eclogite or epidote eclogite with 5.0 vol% epidote and the AK135 model is apparently not in the region of high-velocity anomalies of the Farallon plate (Fig. 5), which does not explain the high-velocity anomalies observed in the Farallon plate at 100–300 km. On the contrary, the velocity difference between the zoisite eclogite (16.0 vol% zoisite) and the AK135 model is consistent with the high-velocity anomalies observed in the Farallon plate. Thus, as to the analysis above, we conclude that the typical zoisite eclogite with 16.0 vol% zoisite (~61.0 vol% omphacite, ~23.0 vol% garnet, and ~16.0 vol% zoisite) is one of the possible reasons for the high-velocity anomalies of the Farallon plate at 100–300 km depths.

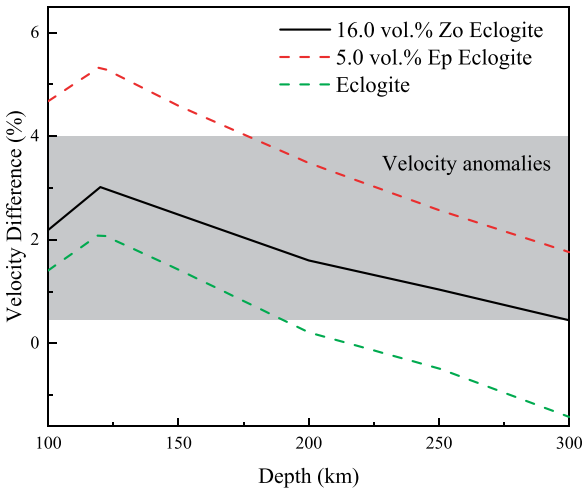

Figure 5. Velocity differences among the three eclogite petrological models along the Farallon slab geotherm and the AK135 model at 100–300 km depths are shown. The light gray region indicates the range of seismic velocity anomalies of the Farallon plate at depths of 100–300 km. The black solid line indicates the velocity difference between 16.0 vol% zoisite eclogite and AK135, while the red dashed line indicates the velocity difference between 5.0 vol% epidote eclogite and AK135. The green dashed line indicates the velocity difference between eclogite and AK135.

CONCLUSION

The thermoelastic properties and stability of zoisite at high temperatures and pressures (up to 700 K and 24.8 GPa) were studied by synchrotron radiation SC-XRD. Our results show that zoisite is stable under the *P-T* conditions in this study, which indicates that zoisite is capable of carrying water into ~300 km depth under cold subduction conditions. The thermal EoS parameters of zoisite, $K_0 = 134.7(8)$ GPa, $\alpha_{0V} = 1.9(7) \times 10^{-5}$ K^{-1}, $\alpha_{1V} = 3(2) \times 10^{-5}$ K^{-2}, and $(\partial K/\partial T)_P = -0.011(4)$ GPa/K, were obtained by fitting the *P-V-T* data using the BM-EoS

Downloaded from http://pubs.geoscienceworld.org/gsa/gsabulletin/article-pdf/135/5-6/1178/5827011/b36479.1.pdf
by Argonne National Laboratory user

combined with Fei's thermal expansion model, which has been used to calculate the density and bulk sound velocity of zoisite and zoisite eclogite along the Farallon plate geotherm. Finally, based on the calculated density and bulk sound velocity profiles of zoisite eclogite along the Farallon plate geotherm, we conclude that zoisite could carry water to depths of ~300 km within cold subducting slabs, and the typical zoisite eclogite with ~61.0 vol% omphacite, ~23.0 vol% garnet, and ~16.0 vol% zoisite could be one of the reasons for the high-velocity anomalies at depths of 100–300 km in the Farallon plate.

ACKNOWLEDGMENTS

This project was funded by the National Natural Science Foundation of China (U2032118, 42172048, and 41802043), the Youth Innovation Promotion Association of the Chinese Academy of Sciences (Dawei Fan, 2018434), the Chinese Academy of Sciences "Light of West China" Program (2019), and the Guizhou Provincial Science and Technology Projects (QKHJC-ZK[2021]ZD042). The experiments were performed at 13-BM-C station, GeoSoilEnviroCARS, Advanced Photon Source (APS), at Argonne National Laboratory, Lemont, Illinois, USA. The use of the gas-loading system is supported by COMPRES and GeoSoilEnviroCARS. GeoSoilEnviroCARS is supported by the National Science Foundation—Earth Sciences (EAR-1634415) and the Department of Energy—Geosciences (DE-FG02-94ER14466). COMPRES is under National Science Foundation Cooperative Agreement EAR-1661511. Use of the Advanced Photon Source was supported by the U.S. Department of Energy, Office of Science, Office of Basic Energy Sciences, under contract no. DE-AC02-06CH11357. We acknowledge Sergey N. Tkachev for assistance with gas loading and Dongyang Ju for guiding the calculation of bulk sound velocity. The authors declare no competing financial interests.

REFERENCES CITED

Alvaro, M., Angel, R.J., and Cámara, F., 2012, High-pressure behavior of zoisite: The American Mineralogist, v. 97, p. 1165–1176, https://doi.org/10.2138/am.2012.4014.

Angel, R.J., Bujak, M., Zhao, J., Gatta, G.D., and Jacobsen, S.D., 2007, Effective hydrostatic limits of pressure media for high-pressure crystallographic studies: Journal of Applied Crystallography, v. 40, p. 26–32, https://doi.org/10.1107/S0021889806045523.

Angel, R.J., Gonzalez-Platas, J., and Alvaro, M., 2014, EosFit7c and a Fortran module (library) for equation of state calculations: Zeitschrift für Kristallographie—Crystalline Materials, v. 229, https://doi.org/10.1515/zkri-2013-1711.

Ballaran, T.B., and Angel, R.J., 2003, Equation of state and high-pressure phase transitions in lawsonite: European Journal of Mineralogy, v. 15, p. 241–246, https://doi.org/10.1127/0935-1221/2003/0015-0241.

Bina, C.R., and Navrotsky, A., 2000, Possible presence of high-pressure ice in cold subducting slabs: Nature, v. 408, p. 844–847, https://doi.org/10.1038/35048555.

Bustamante, A., Bustamante, C., Cardona, A., Juliani, C., and Pereira da Silva, S., 2021, Jambaló blueschist and greenschist protoliths in the Central Cordillera of the Colombian Andes and their tectonic implications for Late Cretaceous Caribbean–South American interactions: Journal of South American Earth Sciences, v. 107, https://doi.org/10.1016/j.jsames.2020.102977.

Chen, H.W., Leinenweber, K., Prakapenka, V., Kunz, M., Bechtel, H.A., Liu, Z.X., and Shim, S.H., 2020, Phase transformation of hydrous ringwoodite to the lower-mantle phases and the formation of dense hydrous silica: The American Mineralogist, v. 105, p. 1342–1348, https://doi.org/10.2138/am-2020-7261.

Chen, Y.X., Zheng, Y.F., Gao, X.Y., and Hu, Z., 2014, Multiphase solid inclusions in zoisite-bearing eclogite: Evidence for partial melting of ultrahigh-pressure metamorphic rocks during continental collision: Lithos, v. 200–201, p. 1–21, https://doi.org/10.1016/j.lithos.2014.04.004.

Cheng, H., Liu, Y., Vervoort, J.D., and Lu, H., 2015, Combined U-Pb, Lu-Hf, Sm-Nd and Ar-Ar multichronometric dating on the Bailang eclogite constrains the closure timing of the Paleo-Tethys Ocean in the Lhasa terrane, Tibet: Gondwana Research, v. 28, p. 1482–1499, https://doi.org/10.1016/j.gr.2014.09.017.

Comodi, P., and Zanazzi, P.F., 1997, The pressure behavior of clinozoisite and zoisite: An X-ray diffraction study: The American Mineralogist, v. 82, p. 61–68, https://doi.org/10.2138/am-1997-1-208.

Delany, J.M., and Helgeson, H.C., 1978, Calculation of the thermodynamic consequences of dehydration in subducting oceanic crust to 100 kb and & >800 degrees C: American Journal of Science, v. 278, p. 638–686, https://doi.org/10.2475/ajs.278.5.638.

Dong, Y.L., Wang, B.D., Zhao, W.X., Yang, T.N., and Xu, J.F., 2016, Discovery of eclogite in the Bangong Co–Nujiang ophiolitic mélange, central Tibet, and tectonic implications: Gondwana Research, v. 35, p. 115–123, https://doi.org/10.1016/j.gr.2016.03.010.

Dziewonski, A.M., and Anderson, D.L., 1981, Preliminary reference Earth model: Physics of the Earth and Planetary Interiors, v. 25, p. 297–356, https://doi.org/10.1016/0031-9201(81)90046-7.

English, J.M., Johnston, S.T., and Wang, K., 2003, Thermal modelling of the Laramide orogeny: Testing the flat-slab subduction hypothesis: Earth and Planetary Science Letters, v. 214, p. 619–632, https://doi.org/10.1016/S0012-821X(03)00399-6.

Fei, Y.W., Ricolleau, A., Frank, M., Mibe, K., Shen, G.Y., and Prakapenka, V., 2007, Toward an internally consistent pressure scale: Proceedings of the National Academy of Sciences of the United States of America, v. 104, p. 9182–9186, https://doi.org/10.1073/pnas.0609013104.

Feng, P., Wang, L., Brown, M., Johnson, T.E., Kylander-Clark, A., and Piccoli, P.M., 2021, Partial melting of ultrahigh-pressure eclogite by omphacite-breakdown facilitates exhumation of deeply-subducted crust: Earth and Planetary Science Letters, v. 554, https://doi.org/10.1016/j.epsl.2020.116664.

Forneris, J.F., and Holloway, J.R., 2003, Phase equilibria in subducting basaltic crust: Implications for H_2O release from the slab: Earth and Planetary Science Letters, v. 214, p. 187–201, https://doi.org/10.1016/S0012-821X(03)00305-4.

Gatta, G.D., Merlini, M., Lee, Y., and Poli, S., 2011, Behavior of epidote at high pressure and high temperature: A powder diffraction study up to 10 GPa and 1,200 K: Physics and Chemistry of Minerals, v. 38, p. 419–428, https://doi.org/10.1007/s00269-010-0415-y.

Grevel, K.-D., Nowlan, E.U., Fasshauer, D.W., and Burchard, M., 2000, In situ X-ray diffraction investigation of lawsonite and zoisite at high pressures and temperatures: The American Mineralogist, v. 85, p. 206–216, https://doi.org/10.2138/am-2000-0120.

Hacker, B.R., and Abers, G.A., 2004, Subduction factory 3: An Excel worksheet and macro for calculating the densities, seismic wave speeds, and H_2O contents of minerals and rocks at pressure and temperature: Geochemistry, Geophysics, Geosystems, v. 5, https://doi.org/10.1029/2003GC000614.

Hacker, B.R., Abers, G.A., and Peacock, S.M., 2003, Subduction factory 1. Theoretical mineralogy, densities, seismic wave speeds, and H_2O contents: Journal of Geophysical Research: Solid Earth, v. 108, https://doi.org/10.1029/2001JB001127.

Hernández-Uribe, D., and Palin, R.M., 2019, Catastrophic shear-removal of subcontinental lithospheric mantle beneath the Colorado Plateau by the subducted Farallon slab: Scientific Reports, v. 9, 8153, https://doi.org/10.1038/s41598-019-44628-y.

Hofmeister, A.M., and Mao, H.k., 2002, Redefinition of the mode Grüneisen parameter for polyatomic substances and thermodynamic implications: Proceedings of the National Academy of Sciences of the United States of America, v. 99, p. 559–564, https://doi.org/10.1073/pnas.241631698.

Holland, T.J.B., and Powell, R., 1990, An enlarged and updated internally consistent thermodynamic dataset with uncertainties and correlations: The system K_2O–Na_2O–CaO–MgO–MnO–FeO–Fe_2O_3–Al_2O_3–TiO_2–SiO_2–C–H_2–O_2: Journal of Metamorphic Geology, v. 8, p. 89–124, https://doi.org/10.1111/j.1525-1314.1990.tb00458.x.

Holland, T.J.B., Redfern, S.A.T., and Pawley, A.R., 1996, Volume behavior of hydrous minerals at high pressure and temperature; II, Compressibilities of lawsonite, zoisite, clinozoisite, and epidote: The American Mineralogist, v. 81, p. 341–348, https://doi.org/10.2138/am-1996-3-408.

Huang, S.J., Xu, J.G., Chen, C.F., Li, B., Ye, Z.L., Chen, W., Kuang, Y., Fan, D., Zhou, W., and Ma, M., 2020, Topaz, a potential volatile-carrier in cold subduction zone: Constraint from synchrotron X-ray diffraction and Raman spectroscopy at high temperature and high pressure: Minerals, v. 10, p. 780, https://doi.org/10.3390/min10090780.

Huang, S.J., Xu, J.G., Liu, D.R., Li, B., Ye, Z.L., Chen, W., Kuang, Y., Chi, F., Fan, D., Ma, M., and Zhou, W., 2021, Stability and thermoelasticity of diaspore by synchrotron X-ray diffraction and Raman spectroscopy: Frontiers of Earth Science, v. 9, https://doi.org/10.3389/feart.2021.752566.

Jiang, F.M., Majzlan, J., Speziale, S., He, D.W., and Duffy, T.S., 2008, Single-crystal elasticity of diaspore, AlOOH, to 12 GPa by Brillouin scattering: Physics of the Earth and Planetary Interiors, v. 170, p. 221–228, https://doi.org/10.1016/j.pepi.2008.05.011.

Kantor, I., Prakapenka, V., Kantor, A., Dera, P., Kurnosov, A., Sinogeikin, S., Dubrovinskaia, N., and Dubrovinsky, L., 2012, BX90: A new diamond anvil cell design for X-ray diffraction and optical measurements: The Review of Scientific Instruments, v. 83, https://doi.org/10.1063/1.4768541.

Kennett, B.L.N., Engdahl, E.R., and Buland, R., 1995, Constraints on seismic velocities in the Earth from traveltimes: Geophysical Journal International, v. 122, p. 108–124, https://doi.org/10.1111/j.1365-246X.1995.tb03540.x.

Klotz, S., Chervin, J.C., Munsch, P., and Le Marchand, G., 2009, Hydrostatic limits of 11 pressure transmitting media: Journal of Physics. D, Applied Physics, v. 42, p. 7, https://doi.org/10.1088/0022-3727/42/7/075413.

Lempart, M., Derkowski, A., Straczek, T., and Kapusta, C., 2020, Systematics of H_2 and H_2O evolved from chlorites during oxidative dehydrogenation: The American Mineralogist, v. 105, p. 932–944, https://doi.org/10.2138/am-2020-7326.

Levander, A., Schmandt, B., Miller, M.S., Liu, K., Karlstrom, K.E., Crow, R.S., Lee, C.-T.A., and Humphreys, E.D., 2011, Continuing Colorado plateau uplift by delamination-style convective lithospheric downwelling: Nature, v. 472, p. 461–465, https://doi.org/10.1038/nature10001.

Li, B., Xu, J.G., Zhang, D.Z., Ye, Z.L., Huang, S.J., Fan, D.W., Zhou, W., and Xie, H., 2021, Thermoelasticity and stability of natural epidote at high pressure and high temperature: Implications for water transport during cold slab subduction: Geoscience Frontiers, v. 12, https://doi.org/10.1016/j.gsf.2020.05.022.

Li, X.P., Zheng, Y.F., Wu, Y.B., Chen, F.K., Gong, B., and Li, Y.L., 2004, Low-T eclogite in the Dabie terrane of China: Petrological and isotopic constraints on fluid activity and radiometric dating: Contributions to Mineralogy and Petrology, v. 148, p. 443–470, https://doi.org/10.1007/s00410-004-0616-9.

Li, Z., Yang, J., Xu, Z., Li, T., Xu, X., Ren, Y., and Robinson, P.T., 2009, Geochemistry and Sm–Nd and Rb–Sr isotopic composition of eclogite in the Lhasa terrane, Tibet, and its geological significance: Lithos, v. 109, p. 240–247, https://doi.org/10.1016/j.lithos.2009.01.004.

Li, Z., Li, Y., Wijbrans, J.R., Yang, Q., Qiu, H.-N., and Brouwer, F.M., 2018, Metamorphic P-T path differences between the two UHP terranes of Sulu Orogen, Eastern China: Petrologic comparison between eclogites from

Downloaded from http://pubs.geoscienceworld.org/gsa/gsabulletin/article-pdf/135/5-6/1178/5827011/b36479.1.pdf
by Argonne National Laboratory user

Donghai and Rongcheng: Journal of Earth Science, v. 29, p. 1151–1166, https://doi.org/10.1007/s12583-018-0845-x.

Liu, Q., Jin, Z., and Zhang, J., 2009, An experimental study of dehydration melting of phengite-bearing eclogite at 1.5–3.0 GPa: Chinese Science Bulletin, v. 54, p. 2090–2100, https://doi.org/10.1007/s11434-009-0140-4.

Liu, Y.H., Yang, H.J., Zhang, J., Shau, Y.H., Chu, M.F., Iizuka, Y., and Yu, S.C., 2010, Kyanite formation and element fractionation in the high-Al eclogites from the Sulu UHP metamorphic terrane: Diqiu Kexue Jikan, v. 21, p. 277–298, https://doi.org/10.3319/TAO.2009.06.12.01(TT).

Mans, W., Zhang, J.S., Hao, M., Smyth, J.R., Zhang, D.Z., Finkelstein, G.J., and Dera, P., 2019, Hydrogen effect on the sound velocities of upper mantle omphacite: Minerals, v. 9, https://doi.org/10.3390/min9110690.

Mao, Z., Jiang, F.M., and Duffy, T.S., 2007, Single-crystal elasticity of zoisite $Ca_2Al_3Si_3O_{12}(OH)$ by Brillouin scattering: The American Mineralogist, v. 92, p. 570–576, https://doi.org/10.2138/am.2007.2329.

Marot, M., Monfret, T., Gerbault, M., Nolet, G., Ranalli, G., and Pardo, M., 2014, Flat versus normal subduction zones: A comparison based on 3-D regional traveltime tomography and petrological modelling of central Chile and western Argentina (29°–35°S): Geophysical Journal International, v. 199, p. 1633–1654, https://doi.org/10.1093/gji/ggu355.

Newton, R.C., and Kennedy, G.C., 1963, Some equilibrium reactions in the join $CaAl_2Si_2O_8$-H_2O: Journal of Geophysical Research, v. 68, p. 2967–2983, https://doi.org/10.1029/JZ068i010p02967.

Nishi, M., Kubo, T., and Kato, T., 2009, Metastable transformations of eclogite to garnetite in subducting oceanic crust: Journal of Mineralogical and Petrological Sciences, v. 104, p. 192–198, https://doi.org/10.2465/jmps.080929.

Nishihara, Y., Takahashi, E., Matsukage, K., and Kikegawa, T., 2003, Thermal equation of state of omphacite: The American Mineralogist, v. 88, p. 80–86, https://doi.org/10.2138/am-2003-0110.

Pavlis, G.L., Sigloch, K., Burdick, S., Fouch, M.J., and Vernon, F.L., 2012, Unraveling the geometry of the Farallon plate: Synthesis of three-dimensional imaging results from USArray: Tectonophysics, v. 532–535, p. 82–102, https://doi.org/10.1016/j.tecto.2012.02.008.

Pawley, A.R., Redfern, S.A.T., and Holland, T.J.B., 1996, Volume behavior of hydrous minerals at high pressure and temperature. 1. Thermal expansion of lawsonite, zoisite, clinozoisite, and diaspore: The American Mineralogist, v. 81, p. 335–340, https://doi.org/10.2138/am-1996-3-407.

Pawley, A.R., Chinnery, N.J., and Clark, S.M., 1998, Volume measurements of zoisite at simultaneously elevated pressure and temperature: The American Mineralogist, v. 83, p. 1030–1036, https://doi.org/10.2138/am-1998-9-1011.

Poli, S., and Schmidt, M.W., 1995, H_2O transport and release in subduction zones: Experimental constraints on basaltic and andesitic systems: Journal of Geophysical Research: Solid Earth, v. 100, p. 22,299–22,314, https://doi.org/10.1029/95JB01570.

Poli, S., and Schmidt, M.W., 1998, The high-pressure stability of zoisite and phase relationships of zoisite-bearing assemblages: Contributions to Mineralogy and Petrology, v. 130, p. 162–175, https://doi.org/10.1007/s004100050357.

Roecker, S.W., 1982, Velocity structure of the Pamir-Hindu Kush Region: Possible evidence of subducted crust: Journal of Geophysical Research: Solid Earth, v. 87, p. 945–959, https://doi.org/10.1029/JB087iB02p00945.

Schmidt, M.W., and Poli, S., 1994, The stability of lawsonite and zoisite at high pressures: Experiments in CASH to 92 kbar and implications for the presence of hydrous phases in subducted lithosphere: Earth and Planetary Science Letters, v. 124, p. 105–118, https://doi.org/10.1016/0012-821X(94)00080-8.

Selverstone, J., Pun, A., and Condie, K.C., 1999, Xenolithic evidence for Proterozoic crustal evolution beneath the Colorado Plateau: Geological Society of America Bulletin, v. 111, p. 590–606, https://doi.org/10.1130/0016-7606(1999)111<0590:XEFPCE>2.3.CO;2.

Sigloch, K., 2011, Mantle provinces under North America from multifrequency P wave tomography: Geochemistry, Geophysics, Geosystems, v. 12, https://doi.org/10.1029/2010GC003421.

Suzuki, I., and Anderson, O.L., 1983, Elasticity and thermal expansion of a natural garnet up to 1000 K: Journal of Physics of the Earth, v. 31, p. 125–138, https://doi.org/10.4294/jpe1952.31.125.

Thompson, E.C., Davis, A.H., Brauser, N.M., Liu, Z.X., Prakapenka, V.B., and Campbell, A.J., 2020, Phase transitions in epsilon-FeOOH at high pressure and ambient temperature: The American Mineralogist, v. 105, p. 1769–1777, https://doi.org/10.2138/am-2020-7468.

Urann, B.M., Dick, H.J.B., Parnell-Turner, R., and Casey, J.F., 2020, Recycled arc mantle recovered from the Mid-Atlantic Ridge: Nature Communications, v. 11, p. 3887, https://doi.org/10.1038/s41467-020-17604-8.

Usui, T., Nakamura, E., Kobayashi, K., Maruyama, S., and Helmstaedt, H., 2003, Fate of the subducted Farallon plate inferred from eclogite xenoliths in the Colorado Plateau: Geology, v. 31, p. 589–592, https://doi.org/10.1130/0091-7613(2003)031<0589:FOTSFP>2.0.CO;2.

Usui, T., Eizo, N., and Herwart, H., 2006, Petrology and geochemistry of eclogite xenoliths from the Colorado Plateau: Implications for the evolution of subducted oceanic crust: Journal of Petrology, v. 47, p. 929–964, https://doi.org/10.1093/petrology/egi101.

Usui, T., Kobayashi, K., Nakamura, E., and Helmstaedt, H., 2007, Trace element fractionation in deep subduction zones inferred from a lawsonite-eclogite xenolith from the Colorado Plateau: Chemical Geology, v. 239, p. 336–351, https://doi.org/10.1016/j.chemgeo.2006.08.009.

Van der Lee, S., and Nolet, G., 1997, Seismic image of the subducted trailing fragments of the Farallon plate: Nature, v. 386, p. 266–269, https://doi.org/10.1038/386266a0.

Wang, Y., Forsyth, D.W., Rau, C.J., Carriero, N., Schmandt, B., Gaherty, J.B., and Savage, B., 2013, Fossil slabs attached to unsubducted fragments of the Farallon plate: Proceedings of the National Academy of Sciences of the United States of America, v. 110, p. 5342–5346, https://doi.org/10.1073/pnas.1214880110.

Wei, C., Wang, W., Clarke, G.L., Zhang, L., and Song, S., 2009, Metamorphism of high/ultrahigh-pressure pelitic–felsic schist in the south Tianshan Orogen, NW China: Phase equilibria and P-T path: Journal of Petrology, v. 50, p. 1973–1991, https://doi.org/10.1093/petrology/egp064.

Winkler, B., Milman, V., and Nobes, R.H., 2001, A theoretical investigation of the relative stabilities of Fe-free clinozoisite and orthozoisite: Physics and Chemistry of Minerals, v. 28, p. 471–474, https://doi.org/10.1007/s002690100177.

Xiao, Y., Lavis, S., Niu, Y., Pearce, J.A., Li, H., Wang, H., and Davidson, J., 2012, Trace-element transport during subduction-zone ultrahigh-pressure metamorphism: Evidence from western Tianshan, China: Geological Society of America Bulletin, v. 124, p. 1113–1129, https://doi.org/10.1130/B30523.1.

Xu, J., Zhang, D., Fan, D., Dera, P.K., Shi, F., and Zhou, W., 2019a, Thermoelastic properties of eclogitic garnets and omphacites: Implications for deep subduction of oceanic crust and density anomalies in the upper mantle: Geophysical Research Letters, v. 46, p. 179–188, https://doi.org/10.1029/2018GL081170.

Xu, J.G., Zhang, D.Z., Fan, D.W., Wu, X., Shi, F., and Zhou, W.G., 2019b, Compressional behavior of natural eclogitic zoisite by synchrotron X-ray single-crystal diffraction to 34 GPa: Physics and Chemistry of Minerals, v. 46, p. 333–341, https://doi.org/10.1007/s00269-018-1006-6.

Xu, J.G., Zhang, D.Z., Tkachev, S.N., and Dera, P.K., 2022, Partnership for eXtreme Xtallography (PX^2)—A state-of-the-art experimental facility for extreme-conditions crystallography: A case study of pressure-induced phase transition in natural ilvaite: Matter and Radiation at Extremes, v. 7, 028401, https://doi.org/10.1063/5.0075795.

Yang, C.P., Inoue, T., Yamada, A., Kikegawa, T., and Ando, J., 2014, Equation of state and phase transition of antigorite under high pressure and high temperature: Physics of the Earth and Planetary Interiors, v. 228, p. 56–62, https://doi.org/10.1016/j.pepi.2013.07.008.

Yang, W.C., 2009, The crust and upper mantle of the Sulu UHPM belt: Tectonophysics, v. 475, p. 226–234, https://doi.org/10.1016/j.tecto.2009.02.048.

Ye, Z.L., Fan, D.W., Tang, Q.Z., Xu, J.G., Zhang, D.Z., and Zhou, W.G., 2021, Constraining the density evolution during destruction of the lithospheric mantle in the eastern North China Craton: Gondwana Research, v. 91, p. 18–30, https://doi.org/10.1016/j.gr.2020.12.001.

Zack, T., Rivers, T., Brumm, R., and Kronz, A., 2004, Cold subduction of oceanic crust: Implications from a lawsonite eclogite from the Dominican Republic: European Journal of Mineralogy, v. 16, p. 909–916, https://doi.org/10.1127/0935-1221/2004/0016-0909.

Zhang, D.Z., Dera, P.K., Eng, P.J., Stubbs, J.E., Zhang, J.S., Prakapenka, V.B., and Rivers, M.L., 2017, High pressure single crystal diffraction at PX^2: JoVE: Journal of Visualized Experiments, https://doi.org/10.3791/54660.

Zhang, L., Zhang, L., Lü, Z., Bader, T., and Chen, Z., 2016, Nb–Ta mobility and fractionation during exhumation of UHP eclogite from southwestern Tianshan, China: Journal of Asian Earth Sciences, v. 122, p. 136–157, https://doi.org/10.1016/j.jseaes.2016.03.013.

Zhang, L., Wang, Y., Zhang, L., and Lü, Z., 2019, Ultrahigh pressure metamorphism and tectonic evolution of southwestern Tianshan orogenic belt, China: A comprehensive review, *in* Zhang, L., Zhang, Z., Schertl, H.-P., and Wei. C., eds., HP–UHP Metamorphism and Tectonic Evolution of Orogenic Belts: Geological Society, London, Special Publication 474, p. 133–152, https://doi.org/10.1144/SP474.12.

Zhang, Z.M., Shen, K., Sun, W.D., Liu, Y.S., Liou, J.G., Shi, C., and Wang, J.L., 2008, Fluids in deeply subducted continental crust: Petrology, mineral chemistry and fluid inclusion of UHP metamorphic veins from the Sulu orogen, eastern China: Geochimica et Cosmochimica Acta, v. 72, p. 3200–3228, https://doi.org/10.1016/j.gca.2008.04.014.

Zheng, Y.F., 2009, Fluid regime in continental subduction zones: Petrological insights from ultrahigh-pressure metamorphic rocks: Journal of the Geological Society, v. 166, p. 763–782, https://doi.org/10.1144/0016-76492008-016R.

Zheng, Y.F., 2019, Subduction zone geochemistry: Geoscience Frontiers, v. 10, p. 1223–1254, https://doi.org/10.1016/j.gsf.2019.02.003.

Zheng, Y.F., and Hermann, J., 2014, Geochemistry of continental subduction-zone fluids: Earth, Planets, and Space, v. 66, p. 93, https://doi.org/10.1186/1880-5981-66-93.

Zheng, Y.F., Gao, T.S., Wu, Y.B., Gong, B., and Liu, X.M., 2007, Fluid flow during exhumation of deeply subducted continental crust: Zircon U-Pb age and O-isotope studies of a quartz vein within ultrahigh-pressure eclogite: Journal of Metamorphic Geology, v. 25, p. 267–283, https://doi.org/10.1111/j.1525-1314.2007.00696.x.

Zheng, Y.F., Gao, X.Y., Chen, R.X., and Gao, T.S., 2011, Zr-in-rutile thermometry of eclogite in the Dabie orogen: Constraints on rutile growth during continental subduction-zone metamorphism: Journal of Asian Earth Sciences, v. 40, p. 427–451, https://doi.org/10.1016/j.jseaes.2010.09.008.

Zheng, Y.F., Chen, R.X., Xu, Z., and Zhang, S.B., 2016, The transport of water in subduction zones: Science China Earth Sciences, v. 59, p. 651–682, https://doi.org/10.1007/s11430-015-5258-4.

Science Editor: Brad S. Singer
Associate Editor: Hongping He

Manuscript Received 9 February 2022
Revised Manuscript Received 29 April 2022
Manuscript Accepted 10 June 2022

Printed in the USA

Downloaded from http://pubs.geoscienceworld.org/gsa/gsabulletin/article-pdf/135/5-6/1178/5827011/b36479.1.pdf
by Argonne National Laboratory user